

H₂ dissociation due to collision with He

L. Ohlinger and R. C. Forrey

Department of Physics, Penn State University, Berks Campus, Reading, PA 19610-6009

Teck-Ghee Lee

Department of Physics and Astronomy, University of Kentucky, Lexington, KY 40506

and Physics Division, Oak Ridge National Laboratory, Oak Ridge, TN 37831

P. C. Stancil

Department of Physics and Astronomy, and Center for Simulational Physics,

University of Georgia, Athens, GA 30602

(August 24, 2007)

Abstract

Cross sections for dissociation of H₂ due to collision with He are calculated for highly excited rovibrational states using the quantum mechanical coupled states approximation. An L^2 Sturmian basis set with multiple length scales is used to provide a discrete representation of the H₂ continuum which includes orbiting resonances and a non-resonant background. Cross sections are given over a range of translational energies for both resonant and non-resonant dissociation together with the most important bound state transitions for many different initial states. The results demonstrate that it is possible to compute converged quantum mechanical cross sections using basis sets of modest size. It is found that collision induced dissociation competes with inelastic scattering as a depopulation mechanism for the highly excited states. The relevance of the present calculations to astrophysical models is discussed.

I. INTRODUCTION

The role of hydrogen molecules in a variety of astrophysical environments, including photodissociation regions, star-forming regions, circumstellar shells, and other molecular regions, is far-reaching. Hydrogen molecules are pivotal to establishing the temperature and density structure of the gas and provide diagnostics through emission, absorption, and fluorescence. However, these environments are typically of low density, may be exposed to shocks, and are usually irradiated in the UV by nearby hot stars which likely result in a significant departure from equilibrium for the chemical, ionization, and internal energy state of the gas [1–3]. Therefore, to accurately model these environments, and thereby interpret results from spectroscopic observations, requires a quantitative understanding of a variety of microphysical processes including collisional dissociation and at high density, three-body recombination.

Hydrogen atom recombination in the presence of helium is a fundamental problem that has been studied for over 30 years. The original theoretical approaches [4,5] calculated the rate of stabilization of a steady-state population of H_2 orbiting resonances due to collisions with helium as a third body. The full set of resonances [6–8] was reduced to a set of 6 after energy and lifetime considerations were taken into account. Classical trajectories were computed for the restricted set of resonances and the recombination rate constants were determined. The reverse process of collision-induced dissociation (CID) of H_2 by He was later studied using similar methods based on classical trajectories [9]. More recently, Sakimoto and co-workers have reported results for semiclassical [10] and quantum mechanical [11–14] calculations of CID for $He+H_2$. The quantum mechanical studies assumed either a restricted geometry [11,12] or else a sudden approximation [13,14]. Comparison of the semiclassical and quantum mechanical results have clarified the usefulness of the various approximations that have been applied to the $He+H_2$ system. Because these studies were limited to the ground and low-lying rovibrational states of the molecule, it is not clear what role, if any, the excited and resonant states would play in a kinetic model for this system. The contribution of resonance states to the total dissociation cross section was found to be small for initial

ground state molecules [10]. However, classical trajectory studies [9] predicted a relatively large resonance contribution for excited states and resonant recombination calculations [5] are in good agreement with experiment [15]. Because the efficiency of transitions for large changes of vibrational quantum number is known to be relatively small, it is likely that for many systems, particularly those that are not initially in a Boltzmann distribution of states, the path to dissociation begins with i) a series of upward steps to highly excited levels or ii) electronic excitation via UV photons or energetic electrons followed by fluorescence decay into near dissociative levels of the ground electronic state with the actual dissociation taking place in either case via small quantum jumps into the continuum.

The results of the resonant classical trajectory studies suggest that it would be desirable to perform quantum mechanical calculations for initial excited states which include coupling to both resonant and non-resonant states in the H_2 continuum. This paper describes such calculations for the highest bound vibrational level for a given initial rotational level ranging from 0 to 20. Quasiresonant energy transfer between ro-vibrational bound states has been found for many of these initial levels [16] and we investigate here whether similar transitions may occur for dissociation into the resonant or non-resonant continuum. In the next section, the quantum mechanical method for CID is presented along with details of the numerical parameters. Resulting cross sections from the calculations are presented in Section III. Section IV briefly addresses the astrophysical relevance of the current work and a summary follows in Section V. Atomic units are used throughout unless otherwise noted.

II. THEORY

The atom-diatom Hamiltonian in the center of mass frame is given by

$$H = -\frac{1}{2m} \nabla_r^2 - \frac{1}{2\mu} \nabla_R^2 + v(r) + V_I(r, R, \theta) , \quad (1)$$

where r is the distance between the hydrogen atoms, R is the distance between the helium atom and the center of mass of the diatom, θ is the angle between \vec{r} and \vec{R} , m is the reduced mass of the diatom, and μ is the reduced mass of the helium atom with respect to the diatom.

The three dimensional potential energy surface is separated into a diatomic potential $v(r)$ and an interaction potential $V_I(r, R, \theta)$. As in the case of bound state transitions, the first step in the computation of dissociation cross sections is to find the appropriate set of solutions to the diatomic Schrödinger equation

$$\left[\frac{1}{2m} \frac{d^2}{dr^2} - \frac{j(j+1)}{2m r^2} - v(r) + \epsilon_{vj} \right] \chi_{vj}(r) = 0 , \quad (2)$$

where v and j are the vibrational and rotational quantum numbers for the eigenstate χ_{vj} . We have found previously that transitions between different vibrational and rotational states occur primarily through $\Delta v = \pm 1$ steps for nearly all bound levels of H_2 . Therefore, we consider dissociation from an initial state (v_0, j_0) where v_0 is the quantum number of the last bound vibrational level for the rotational level j_0 . The dissociative continuum is described by positive energy states, often called pseudostates, with $v > v_0$. The bound ro-vibrational wave functions and the positive energy pseudostates are obtained by diagonalization of the diatomic Hamiltonian in the orthonormal Laguerre polynomial $L_n^{(2l+2)}$ basis set

$$\phi_{l,n}(r) = \sqrt{\frac{an!}{(n+2l+2)!}} (ar)^{l+1} \exp(-ar/2) L_n^{(2l+2)}(ar) . \quad (3)$$

A modest basis set ($N \approx 50$) using a single length scale ($a \approx 20$) is capable of providing good estimates for the entire set of bound state energies. The pseudostate spectrum, however, is not constrained by a variational principle and is very sensitive to the number of basis functions and to the length scale. Resonant energies are stable with respect to variations in the length scale over a limited range when the number of functions is held constant. However, the optimal scale factor for one resonance may be quite different than that of another resonance. Therefore, we have found it convenient to use multiple scale factors in order to represent both the resonant and non-resonant continuum states. Tables 1 and 2 show the energies of all the H_2 resonances obtained using the stabilization method with 90 basis functions for each j and a coarse optimization. Our calculations use the fit [17] to the Ad potential of Ref. [8] and we show Schwenke's results for the Ad potential in the tables for comparison. The results are in good agreement for widths below a few wave numbers. For the broad resonances, our basis set is not large enough to accurately determine the

resonance energy so we simply tune the scale parameter to give an energy near the accepted value [8].

The distinction between resonant and non-resonant dissociation is somewhat artificial for the broad resonances in Tables 1 and 2. These resonances, which become important at high energies, could equally be regarded as quadrature points of the non-resonant background. Nevertheless, we will use the term *resonant dissociation* to mean dissociation into one of the resonant states given in Table 1 or 2, and *non-resonant dissociation* to mean dissociation into the background continuum. The total dissociation cross section is then the sum of the resonant and non-resonant contributions, which is equivalent to summing over the full pseudostate spectrum. It is also noteworthy that transitions to long-lived resonances are assumed here to contribute to dissociation, whereas in many kinetic models such states would effectively behave as bound states.

The large number of pseudostates needed to represent the continuum precludes the use of a fully coupled channel method for performing the scattering calculations, particularly at high energies. Therefore, we use the coupled states (CS) approximation to decouple the orbital angular momentum of the atom from the orbital angular momentum of the molecule. In the CS approximation [18,19], the wave function in the body-fixed frame is expanded for total angular momentum J in the set of diatomic eigenstates as

$$\Psi^{J\Omega}(\vec{R}, \vec{r}) = \frac{1}{R} \sum_{v,j} C_{vj}(R) \chi_{vj}(r) Y_{j\Omega}(\theta, 0) , \quad (4)$$

where Ω is the body-fixed projection of both J and j . The centrifugal term in the total Hamiltonian will give diagonal matrix elements proportional to $J(J+1) + j(j+1) - 2\Omega^2$. The CS approximation is made by neglecting the off-diagonal coriolis couplings that arise in the body-fixed frame. Different variations of the CS approximation have been studied by Krems [20] who found that the J -labeled variant introduced by Pack [18] often performs best, however, it does not allow s -wave scattering for rotationally excited states of the diatom. Therefore, we follow our previous work [16] and use the l -labeled variant originally proposed by McGuire and Kouri [19] which assumes that the diagonal eigenvalue of the orbital angular momentum operator \hat{l}^2 is approximated by $l(l+1)$ where l is a conserved quantum number.

This procedure yields the set of coupled equations

$$\left[\frac{d^2}{dR^2} - \frac{l(l+1)}{R^2} + 2\mu E_{vj} \right] C_{vj}(R) = 2\mu \sum_{v',j'} C_{v'j'}(R) \langle vj\Omega | V_I | v'j'\Omega \rangle, \quad (5)$$

where

$$\begin{aligned} \langle vj\Omega | V_I | v'j'\Omega \rangle &= \sum_{\lambda=0}^{\lambda_{max}} (-1)^\Omega [(2j+1)(2j'+1)]^{1/2} \\ &\times \begin{pmatrix} j' & \lambda & j \\ 0 & 0 & 0 \end{pmatrix} \begin{pmatrix} j' & \lambda & j \\ \Omega & 0 & -\Omega \end{pmatrix} \langle \chi_{vj} | V_\lambda | \chi_{v'j'} \rangle, \end{aligned} \quad (6)$$

and V_λ are coefficients for the expansion of the interaction potential in terms of Legendre polynomials P_λ

$$V_I(r, R, \theta) = \sum_{\lambda=0}^{\lambda_{max}} V_\lambda(r, R) P_\lambda(\cos \theta). \quad (7)$$

The (...) denotes a 3- j symbol. Equation (5) shows that the CS formulation requires a set of calculations for each value of Ω . Therefore, the computational effort scales with $\Omega_{max} = j_0$.

The collision cross section is given by

$$\sigma_{vj \rightarrow v'j'} = \frac{\pi}{2\mu E_{vj}(2j+1)} \sum_{J=0}^{J_{max}} (2J+1) \sum_{\Omega=0}^{\Omega_{max}} (2 - \delta_{\Omega 0}) |\delta_{jj'} \delta_{vv'} - S_{vj;v'j'}^{J\Omega}|^2, \quad (8)$$

where $S_{vj;v'j'}^{J\Omega}$ is the scattering matrix and $E_{vj} = E - \epsilon_{vj}$ is the translational energy for state χ_{vj} . The set of coupled equations (5) may be conveniently solved using the general inelastic scattering program MOLSCAT [21]. For H₂ dissociation, the potential energy surface (PES) should provide an accurate representation for large values of H-H separation. The PES of Muchnick and Russek (MR) [22] was recently used for states of H₂ near dissociation [16]. The cross sections were found to be relatively insensitive to changes in the PES for large stretching of the H-H bond where the parametrization of the surface is poorly constrained. Similar tests were performed in the present work for dissociation into the low-energy H-H continuum. Again, the scattering results were found to be insensitive to changes in the PES for large H-H stretching, so we believe that the MR potential should be adequate for the calculations considered here.

For $j_0 \geq 10$, we expect quasis resonant vibration-rotation (QRVR) energy transfer to dominate. This process is characterized by very efficient transitions that follow the specific propensity rule $\Delta j = -2\Delta v$ for highly excited initial states. Therefore, we select basis states such that $j_0 - 10 \leq j \leq j_0 + 10$ with vibrational levels restricted by

$$v_{min}(j) = v_0 - \frac{1}{2}(j - j_0) - m , \quad (9)$$

$$v_{max}(j) = v_0 - \frac{1}{2}(j - j_0) + n . \quad (10)$$

This basis set was also found to be sufficient for $j_0 < 10$ with $j_{min} = 0$ for para-H₂ and $j_{min} = 1$ for ortho-H₂. As described below, we generally use $m = 2$ which allows transitions to the most probable bound states. For low energies before dissociation becomes possible, it is sufficient to set $n = 1$. This gives a total of 44 coupled states and allows the QRVR and non-QRVR bound state transitions to be easily calculated for small J_{max} . This approach worked very well for cold collisions near dissociation [16]. For energies above the dissociation threshold, the value of n must be increased in order to get a good representation of the resonant as well as a few non-resonant background states for each j . Ideally, we would like to increase n until full convergence of the background contribution is achieved, however, the increasingly large value of J_{max} with energy limits what is practical. In the calculations reported in this work, we have used $J_{max} = 50$ for translational energies between 100 and 1,000 cm⁻¹, $J_{max} = 100$ for energies between 1,000 and 10,000 cm⁻¹, and $J_{max} = 200$ for energies between 10,000 and 100,000 cm⁻¹. Each set of calculations gives good agreement at the overlapping boundary. At energies above 100,000 cm⁻¹, it should be possible to match the quantum mechanical calculations to quasi-classical trajectory calculations as has been done previously for bound state transitions [23].

III. RESULTS

In order to see whether the basis set defined by equations (9) and (10) is adequate for dissociation, it is necessary to study the rate of convergence as a function of collision energy. Figure 1 shows the convergence pattern of the resonant and non-resonant dissociation cross

sections for an initial state with $v_0 = 12$ and $j_0 = 10$. The resonant cross sections have been multiplied by 10 in order to provide better visibility. There is a small decrease in the cross sections in going from $m = 1$ to 2 for $n = 3$. Further increase in m yields an even smaller change in the cross sections. This is due to the rapid rate of convergence for the most probable bound state transitions [16]. The convergence rate for the dissociative transitions is somewhat slower, particularly for the non-resonant contribution. Figure 1 shows that the difference between the $n = 5$ and $n = 6$ cross sections is reasonably small. Therefore, we have used $n = 6$ for $j_0 = 0 - 15$ and $n = 5$ for $j_0 = 16 - 20$ with $m = 2$ in both cases. The decrease in n for high j_0 helps to compensate for the increased number of Ω -projections needed in equation (6) and provides a manageable program execution time without introducing a significant loss of accuracy. The total number of coupled states for all calculations considered in this work is then 88 and 99 for $n = 5$ and $n = 6$, respectively.

Figure 2 shows dissociation cross sections to the resonant states of H_2 for an initial state with $v_0 = 12$ and $j_0 = 10$. The relatively large cross section to the $j = 8$ resonance is due to a QRVR transition with $\Delta v = 1$. Other transitions also satisfy the quasis resonant $\Delta j = -2\Delta v$ propensity rule, however, transitions with $|\Delta v| > 1$ have a larger angular momentum gap which produces cross sections that are smaller than that of $j = 8$. The thresholds for dissociation to resonant states with increasing j occur at increasing collision energies as expected from Table 1. At energies above $10,000 \text{ cm}^{-1}$, the smallest contributions to the total resonant cross section come from $j = 4$, $j = 18$, and $j = 20$. These resonances have the largest internal angular momentum gap and their small contribution suggests that the truncation condition $j_0 - 10 \leq j \leq j_0 + 10$ is sufficient for handling dissociation to the resonant states. Figure 3 shows dissociation cross sections to the non-resonant background continuum of H_2 for the same initial state as Figure 2. The contributions from each positive energy pseudostate are summed over v for each j , which provides a convenient quadrature of the background. The $j \leq 10$ contributions dominate the total non-resonant cross section at energies below 1000 cm^{-1} . At higher energies, the $j > 10$ contributions become important and at energies above $10,000 \text{ cm}^{-1}$, the $j = 20$ curve is larger than many of the other curves

which suggests that additional angular momentum states may be needed to achieve full convergence for dissociation into the non-resonant background continuum at high energies.

Figure 4 shows the total cross sections for transitions to bound states, resonant states, and non-resonant continuum states for $j_0 = 7, 10, 15,$ and 20 . The bound state curve in each case includes cross sections for all possible bound state transitions and is dominated at low energies by QRVR energy transfer [16]. The dissociation curves include cross sections for all possible pseudostate transitions, and the total dissociation curve in each case is the sum of the resonant and non-resonant cross sections. For $j_0 = 7$ and $j_0 = 10$, the resonant and non-resonant curves cross near 200 cm^{-1} and 500 cm^{-1} , respectively. As j_0 is increased further, the resonant contribution dominates the dissociation cross section for energies less than $20,000 \text{ cm}^{-1}$. The total dissociation curves for $j_0 = 7$ and $j_0 = 10$ cross the bound state curves around 900 cm^{-1} and 2000 cm^{-1} , respectively. Above these energies, the H_2 molecule is more likely to dissociate than to transition into another bound ro-vibrational level. This crossing point does not occur for the higher j_0 states in (c) and (d) until collision energies approaching $100,000 \text{ cm}^{-1}$ are reached.

Similar analysis was performed for other initial states. Figure 5 shows the resonant dissociation cross sections for para- H_2 with $j_0 \leq 20$. The initial vibrational level v_0 , which corresponds to the most weakly bound state for a given j_0 , is also shown in the legend. Each curve represents a sum of cross sections for all possible resonant transitions for the indicated initial state. The $j_0 = 2$ cross section is the largest for nearly all of the energies shown. The $j_0 = 10$ cross section is also large due to the efficiency of the $j = 8$ transition described above. The $j_0 = 0$ cross section is relatively large at low energy but becomes the smallest of the group at energies above $10,000 \text{ cm}^{-1}$. There does not appear to be any ordered behavior in the remaining curves at low and intermediate energies, and all of the curves for $j_0 \geq 10$ approach nearly the same limiting behavior at high energies. Figure 6 shows the corresponding non-resonant dissociation cross sections for each of the initial states in Figure 5. The contributions from each positive energy pseudostate are summed over both v and j . The resulting curves are found to be smooth functions of energy and are ordered

with increasing j_0 for $j_0 \geq 10$ as shown.

Figures 7 and 8 show the respective resonant and non-resonant dissociation cross sections for ortho-H₂. The curves are comparable to those of para-H₂ although the thresholds tend to be shifted toward higher energies due to the deeper binding energies of the initial states. The $j_0 = 3$ and $j_0 = 7$ resonant cross sections are largest at low and intermediate energies. The efficiency of the $j_0 = 7$ cross section is due to the availability of a QRVR transition to the $j = 5$ resonance. The $j_0 = 1$ resonant cross section is relatively large at low energy but becomes the smallest of the group at high energies, similar to the $j_0 = 0$ cross section for para-H₂. Figure 8 shows that the non-resonant cross sections have smoother and more orderly behavior than the corresponding resonant cross sections, again similar to para-H₂.

The total dissociation cross section for a given initial state is obtained as the sum of the resonant and non-resonant contributions. Likewise, the total bound state cross section is defined to be the sum of cross sections for all possible transitions from a given initial state to a final bound state. In Figures 9 and 10, the total dissociation cross section divided by the total bound state cross section is shown as a function of energy for both para-H₂ and ortho-H₂. The results are presented as ratios in order to see the relative importance of dissociation compared to bound state transitions. For para-H₂, the $j_0 = 2$ curve is largest at all energies. The $j_0 = 10$ curve is also large with a ratio that approaches two at the highest energy shown. All of the curves have a ratio greater than 0.01 for energies above 1000 cm⁻¹ and 0.1 for energies above 2000 cm⁻¹. For ortho-H₂, the $j_0 = 3$ curve is largest at all energies followed by the $j_0 = 7$ and $j_0 = 1$ curves at low energies. The remaining curves show no significant dissociation for energies below 300 cm⁻¹. At this energy, however, the $j_0 = 3$ ratio becomes greater than unity and dissociation becomes preferable to inelastic scattering. A similar cross-over occurs for para-H₂ around 200 cm⁻¹ due to the $j_0 = 2$ contribution.

The results suggest that dissociation is at least as important as inelastic scattering for all j_0 at high energies. At low energies, only states with $j_0 = 0, 1, 2, 3, 7,$ and 10 yield significant dissociation cross sections. The $j_0 = 7$ and $j_0 = 10$ states are particularly interesting because they can make very specific QRVR transitions to the $j = 5$ and $j = 8$ orbiting resonances

prior to dissociation. Dissociation from the $j_0 = 0 - 3$ states is very efficient due to the small energies needed to reach the continuum, however, transitions from these states do not follow a specific propensity rule as in the case of QRVR transitions, and a larger number of final states make a significant contribution to the total dissociation cross section.

IV. ASTROPHYSICAL APPLICATIONS

As discussed in the introduction, the populations of the rovibrational levels of H_2 may be very different from a thermal distribution in, for example, environments which experience considerable external energy input. A particularly important case is the photodissociation region (PDR) which is found in a variety of astrophysical sources [2]. A PDR is produced when gas is irradiated by UV photons from a nearby star or star cluster. This radiation can be very intense with typical intensities thousands of times larger than the interstellar background UV field. The UV radiation can excite H_2 present in the PDR into low-lying electronic states which decay back to the ground state, but into a range of rovibrational levels. The process tends to drive the rovibrational population distribution out of equilibrium. In fact, highly excited rovibrational states of H_2 have been directly observed in a number of PDRs. An illustrative case is the PDR associated with the reflection nebulae NGC 2023 in Orion. McCartney et al. [24] have observed the H_2 fluorescent emission spectrum in the infrared from NGC 2023 for vibrational levels $v = 1 - 12$ and j as high as 16, i.e., states such as $v = 5, j = 16$ and $v = 9, j = 13$ are actually populated. Looking directly at the illuminated star of NGC 2023, HD 37903, with the *Hubble Space Telescope*, Meyer et al. [25] detected UV absorption lines of vibrationally excited H_2 including from $v = 14, j = 0 - 3$ and $v = 13, j = 1 - 5$. Figures 9 and 10 demonstrate that CID competes with bound-bound transitions as a depopulation mechanism for these highly excited states. Future H_2 PDR models, such as those of Draine and Bertoldi [1] and Shaw et al. [3], should include accurate CID rate coefficients to allow for reliable predictions of rovibrational column densities.

V. CONCLUSIONS

The present work reports the results of quantum mechanical coupled states calculations for $\text{He}+\text{H}_2(v_0, j_0)$ where v_0 is the highest bound vibrational level for $j_0 \leq 20$. The results include numerically converged cross sections for transitions to the most probable bound states as well as transitions to the resonant and non-resonant states of the H_2 continuum. The total dissociation cross sections become larger than the total bound state cross sections at high energies for all initial states included in the study. At low energies, only a few initial states yield a significant amount of dissociation. The cross sections for dissociation from excited levels of H_2 are generally much larger than those computed by Sakimoto [10] for the ground state. Therefore, we expect that the dominant pathway for dissociation in many non-equilibrium environments is through a series of upward steps to the highly excited levels followed by small jumps into the continuum or through fluorescence following electronic excitation. The present results demonstrate that it is possible to compute quantum mechanical cross sections for these dissociative transitions using basis sets of modest size. Such basis sets may be used to compute CID cross sections for weakly bound levels of H_2 not considered here (e.g. the 2nd-most weakly bound vibrational level for a given j_0). It should also be possible to use a similar methodology for H_2+H_2 collisions when the dissociating molecule is initially in a highly excited state with the other molecule in either the ground or a low-lying state. Such calculations would be important for various astrophysical applications including those described here and will be undertaken in due course as an extension of the present calculations.

This work was supported by the National Science Foundation Grant No. PHY-0554794 and by NASA Grant No. NNG05GD81G and the NASA Spitzer Space Telescope Theoretical Research Program.

REFERENCES

- [1] B. T. Draine and F. Bertoldi, *Astrophys. J.* **468**, 269 (1996).
- [2] D. J. Hollenbach and A. G. G. M. Tielens, *Rev. Mod. Phys.* **71**, 173 (1999).
- [3] G. Shaw, G. J. Ferland, N. P. Abel, P. C. Stancil, and P. A. M. van Hoof, *Astrophys. J.* **624**, 794 (2005).
- [4] R. E. Roberts, R. B. Bernstein, and C. F. Curtiss, *J. Chem. Phys.* **50**, 5163 (1969).
- [5] P. A. Whitlock, J. T. Muckerman, and R. E. Roberts, *J. Chem. Phys.* **60**, 3658 (1974).
- [6] T. G. Waech and R. B. Bernstein, *J. Chem. Phys.* **46**, 4905 (1967).
- [7] R. J. LeRoy and R. B. Bernstein, *J. Chem. Phys.* **54**, 5114 (1971).
- [8] D. W. Schwenke, *Theor. Chim. Acta* **74**, 381 (1988).
- [9] J. E. Dove and S. Raynor, *Chem. Phys.* **28**, 113 (1978).
- [10] K. Sakimoto, *Chem. Phys.* **236**, 123 (1998); *J. Chem. Phys.* **110**, 11233 (1999); *Chem. Phys.* **249**, 1 (1999); *J. Chem. Phys.* **112**, 5044 (2000).
- [11] K. Nobusada, K. Sakimoto, and K. Onda, *Chem. Phys. Lett.* **216**, 613 (1993); *Chem. Phys. Lett.* **233**, 399 (1995).
- [12] K. Nobusada and K. Sakimoto, *Chem. Phys.* **197**, 147 (1995).
- [13] K. Nobusada and K. Sakimoto, *J. Chem. Phys.* **106**, 9078 (1997).
- [14] K. Sakimoto, *J. Phys. B* **30**, 3881 (1997).
- [15] D. W. Trainor, D. O. Ham, and F. Kauffman, *J. Chem. Phys.* **58**, 4599 (1973).
- [16] A. Mack, T. K. Clark, R. C. Forrey, N. Balakrishnan, T.-G. Lee, and P. C. Stancil, *Phys. Rev. A* **74**, 052718 (2006).
- [17] D. W. Schwenke, *J. Chem. Phys.* **89**, 2076 (1988).
- [18] R. T. Pack, *J. Chem. Phys.* **60**, 633 (1974).

- [19] P. McGuire and D. J. Kouri, *J. Chem. Phys.* **60**, 2488 (1974); P. McGuire, *J. Chem. Phys.* **62**, 525 (1975).
- [20] R. V. Krems, *J. Chem. Phys.* **116**, 4517 (2002); *J. Chem. Phys.* **116**, 4525 (2002).
- [21] J. M. Hutson and S. Green, MOLSCAT computer code, version 14 (1994), distributed by Collaborative Computational Project No.6 of the Engineering and Physical Sciences Research Council (UK).
- [22] P. Muchnick and A. Russek, *J. Chem. Phys.* **100**, 4336 (1994).
- [23] N. Balakrishnan, M. Vieira, J. F. Babb, A. Dalgarno, R. C. Forrey, and S. Lepp, *Astrophysical Journal* **524**, 1122 (1999).
- [24] M. S. K. McCartney, et al. *Mon. Not. R. Astron. Soc.* 307, 315 (1999).
- [25] D. M. Meyer, et al. *Astrophys. J.* 553, L59 (2001).

Table 1: Resonance parameters for para-H₂($X^1\Sigma_g^+$)

j	present		Schwenke	
	a (a.u.)	E (cm ⁻¹)	E (cm ⁻¹)	Γ (cm ⁻¹)
4	20	0.906	0.842	8.4×10^{-6}
8	30	85.94	86.26	1.485
12	50	386.4	380.5	69.49
14	50	475.3	475.8	17.43
16	50	581.8	581.8	2.826
18	50	721.9	721.8	0.509
20	55	917.4	917.2	0.161
22	60	1181.8	1181.6	0.093
24	60	233.88	233.77	1.1×10^{-21}
24	60	1523.7	1523.5	0.083
26	70	600.56	600.44	1.9×10^{-15}
26	70	1948.45	1948.26	0.097
26	70	2508	2695	268
28	70	1062.54	1062.40	2.1×10^{-12}
28	70	2459.50	2459.34	0.124
28	70	2876	3263	264
30	75	1619.65	1619.48	1.4×10^{-10}
30	75	3059.57	3059.40	0.155
30	75	3545	3914	259
32	75	432.70	432.68	6.0×10^{-34}
32	75	2271.31	2271.16	1.8×10^{-9}
32	75	3750.66	3750.57	0.166
32	75	3962	4657	247
34	80	3016.86	3016.77	5.5×10^{-9}
34	80	4535.04	4534.92	0.138
34	80	4800	5497	218
36	90	5414.5	5414.32	0.061
36	90	6120	6443	166
38	90	6795	7506.67	86.46

Table 2: Resonance parameters for ortho-H₂($X^1\Sigma_g^+$)

j	present		Schwenke	
	a (a.u.)	E (cm ⁻¹)	E (cm ⁻¹)	Γ (cm ⁻¹)
5	30	44.49	43.82	15.22
9	40	185.63	191.26	48.28
11	40	211.56	211.48	2.34
13	40	195.39	195.25	4×10^{-3}
15	55	189.95	189.78	3.2×10^{-6}
15	55	683	687	159
17	60	228.83	228.65	3.6×10^{-8}
17	60	888	883	96.3
19	60	331.56	331.40	1.3×10^{-8}
19	60	1105.9	1117.1	59.7
21	65	510.22	510.08	3.7×10^{-8}
21	65	1401.1	1402.69	40.5
23	70	772.19	772.07	2.2×10^{-7}
23	70	1753.6	1751.13	31.2
25	75	1121.86	1121.73	1.3×10^{-6}
25	75	2175.6	2171.1	27.2
27	75	1561.72	1561.58	6.9×10^{-6}
27	75	2665.7	2669.19	25.8
29	80	474.28	474.14	8.2×10^{-25}
29	80	2093.15	2092.99	2.6×10^{-5}
29	80	3249.1	3251.0	25.3
31	85	1061.40	1061.27	1.5×10^{-18}
31	85	2716.92	2716.74	6.6×10^{-5}
31	85	3920.5	3921.4	24.2
33	90	1744.49	1744.44	8.8×10^{-16}
33	90	3433.52	3433.34	1.0×10^{-4}
33	90	4684.8	4685.1	20.9
35	95	4243.37	4243.24	8.3×10^{-5}
35	95	5546.9	5546.8	14.4
37	100	6511.2	6510.9	5.95

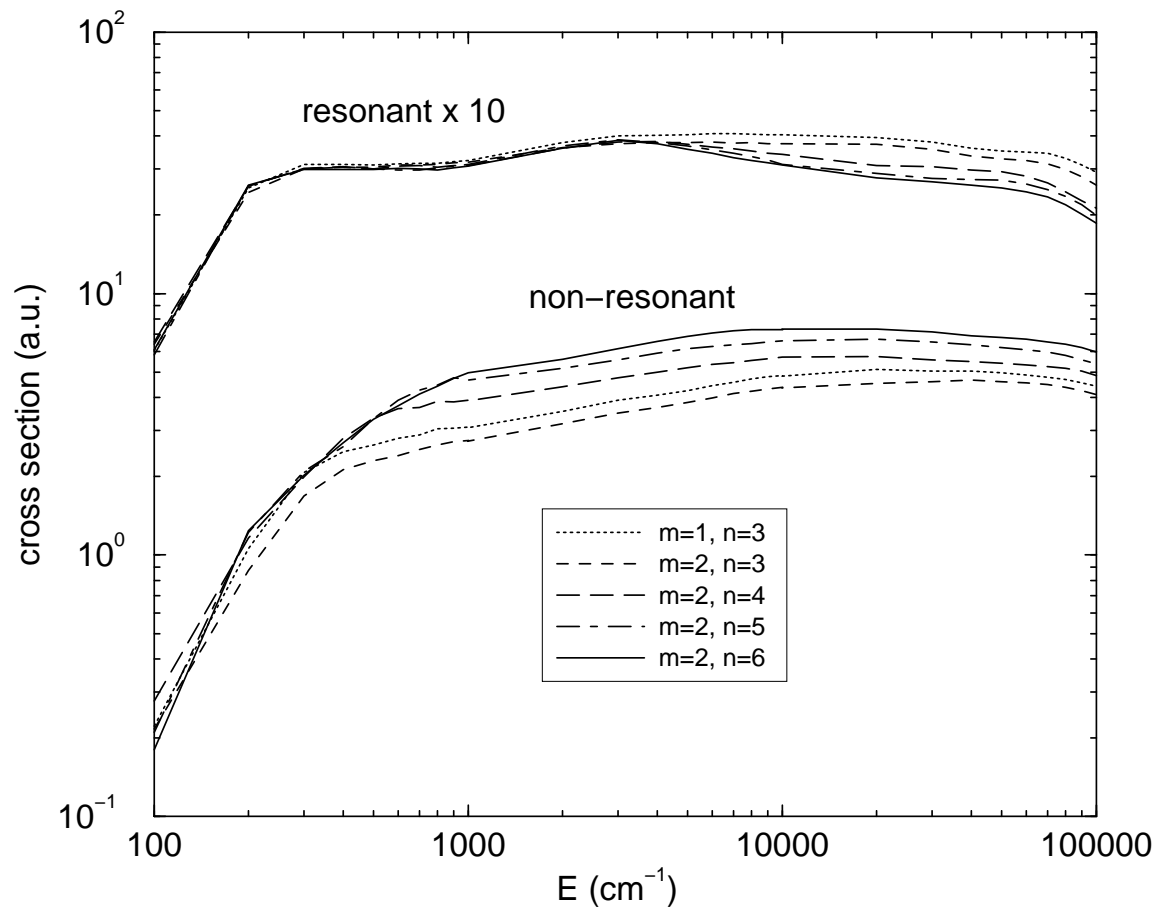


Figure 1: Dissociation cross sections for $\text{He}+\text{H}_2(v_0 = 12, j_0 = 10)$. The resonant cross sections have been multiplied by 10 for better visibility. The convergence rate for the resonant cross sections appears to be faster than for the non-resonant background, particularly at low energy. Satisfactory convergence is obtained for both contributions when $m = 2$ and $n = 6$.

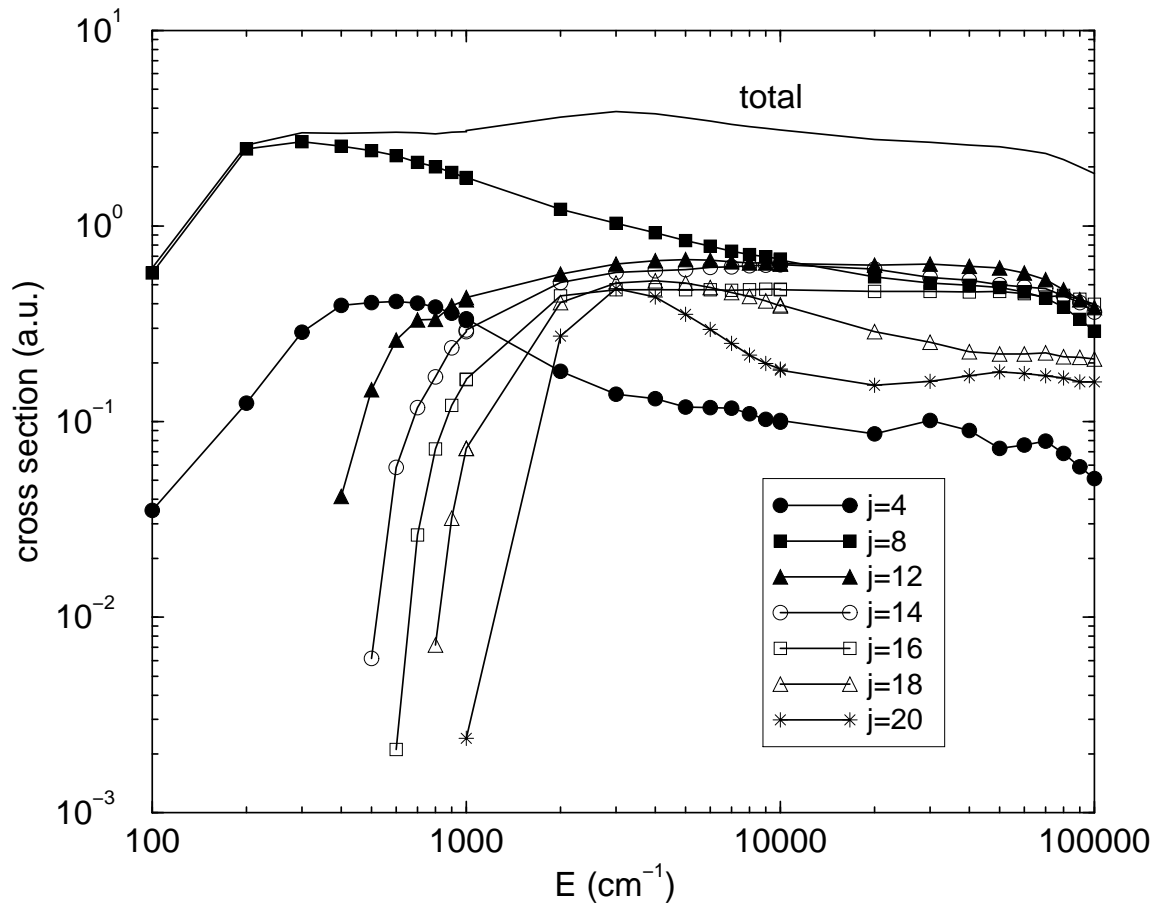


Figure 2: Resonant dissociation cross sections for $\text{He}+\text{H}_2(v_0 = 12, j_0 = 10)$. The relatively large $j = 8$ cross section is due to QRVR $\Delta j = -2\Delta v$ energy transfer. The total cross section is the sum of the curves and is the same as the $m = 2$ and $n = 6$ resonant cross section in Figure 1.

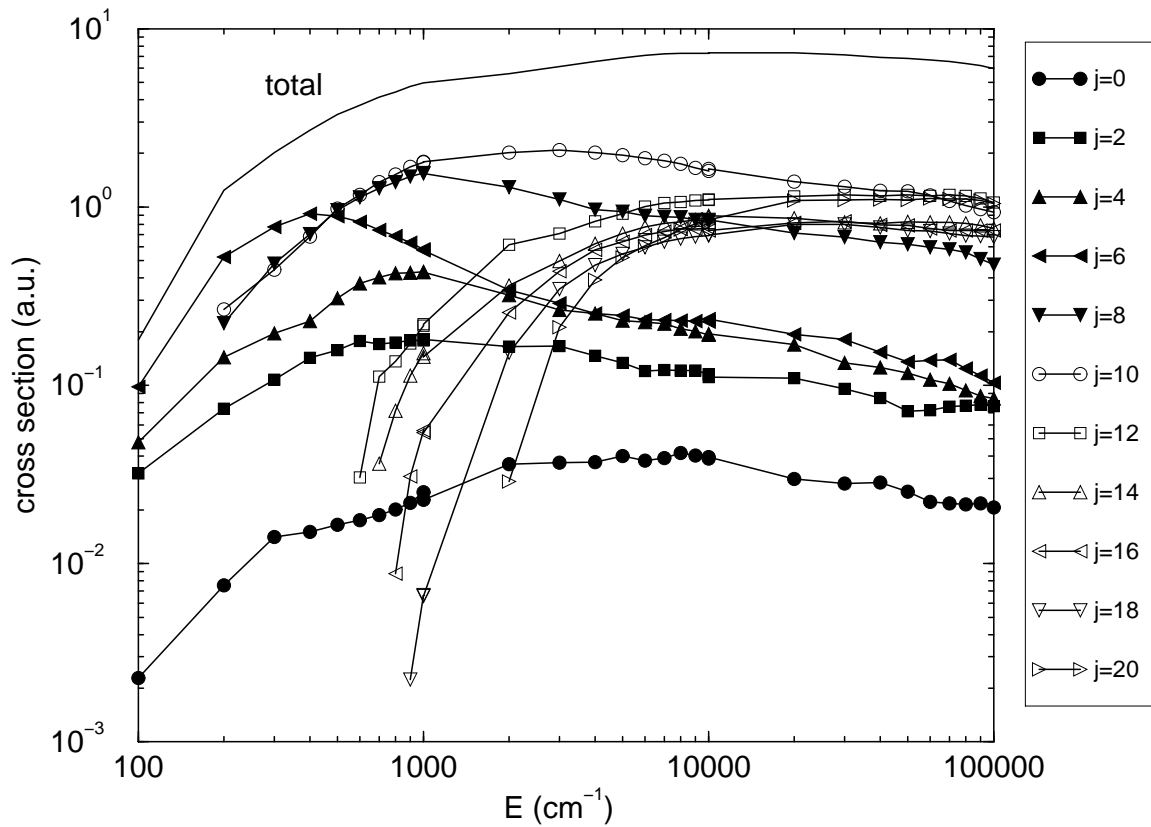


Figure 3: Non-resonant dissociation cross sections for $\text{He}+\text{H}_2(v_0 = 12, j_0 = 10)$. The total cross section is the sum of the curves and is the same as the $m = 2$ and $n = 6$ non-resonant cross section in Figure 1.

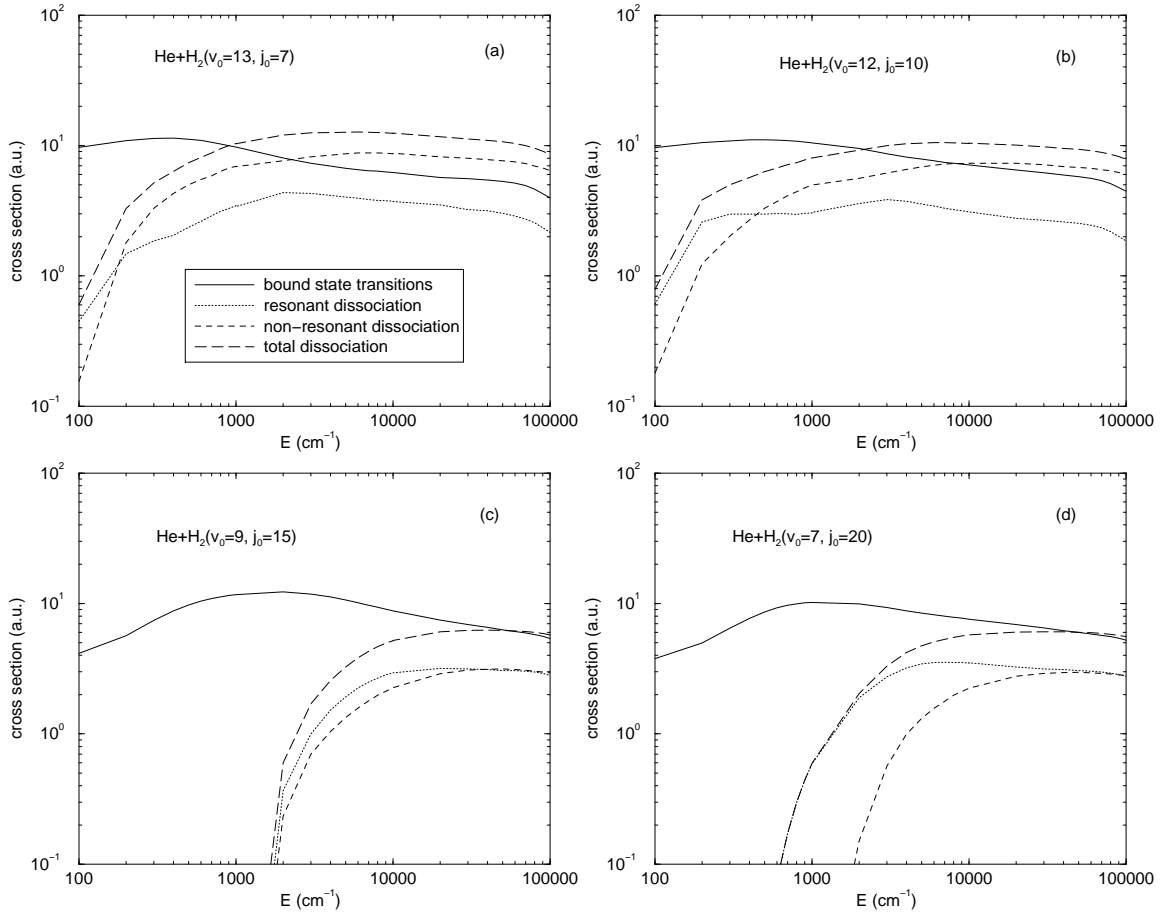


Figure 4: Total cross sections for $\text{He}+\text{H}_2(v_0, j_0)$ for four different initial states. The curves in all four panels are defined the same as in (a). The bound state and dissociation curves include contributions from all possible bound state and pseudostate transitions, respectively.

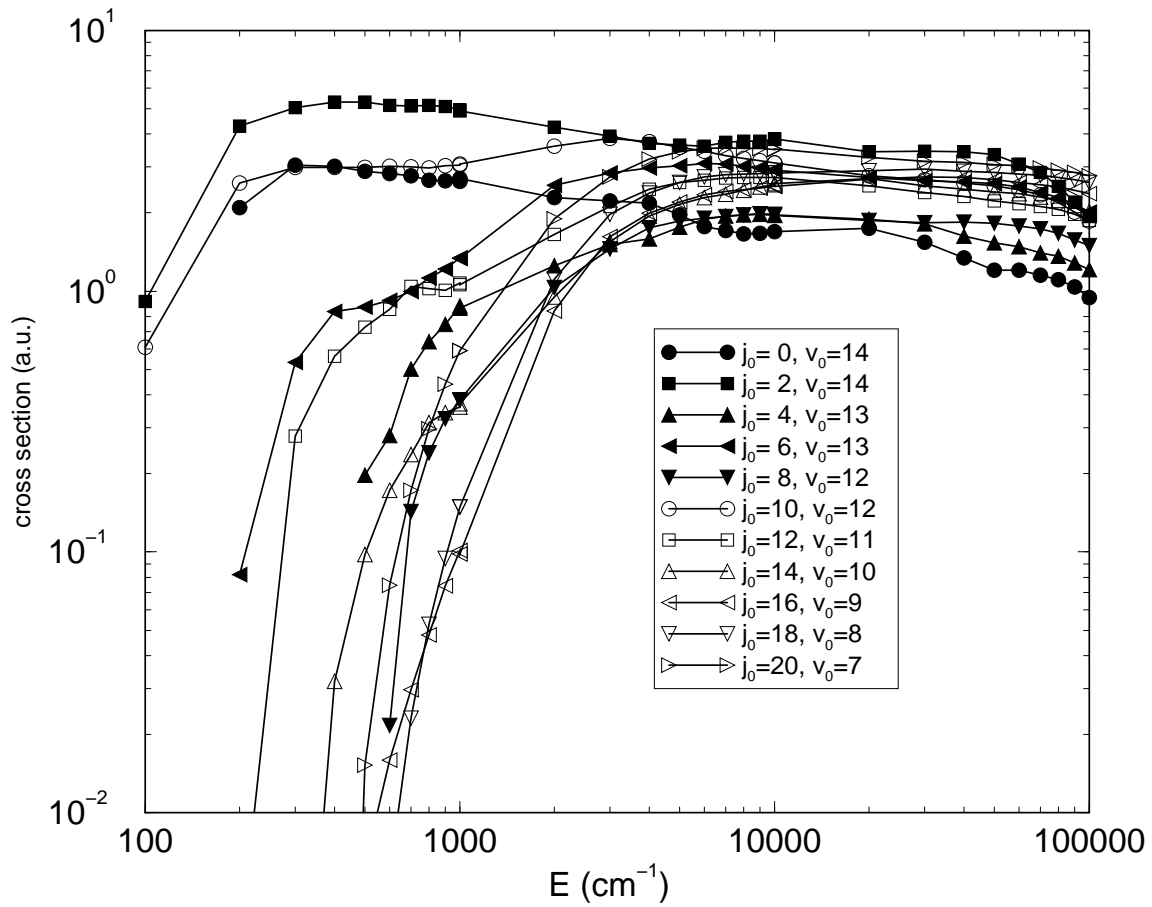


Figure 5: Resonant dissociation cross sections for He collisions with para-H₂. Each curve represents a sum of all possible resonant cross sections for the indicated initial state.

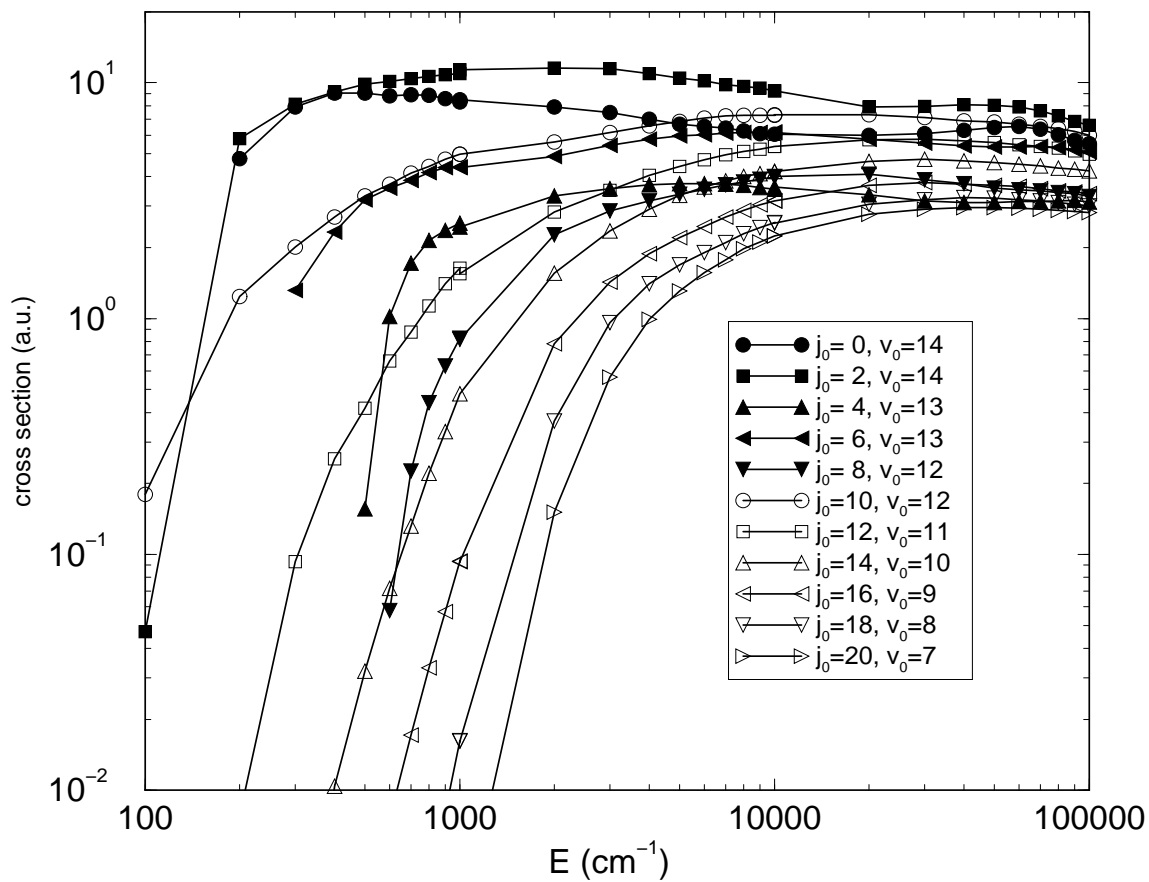


Figure 6: Non-resonant dissociation cross sections for He collisions with para-H₂. Each curve represents a sum of all possible non-resonant cross sections for the indicated initial state.

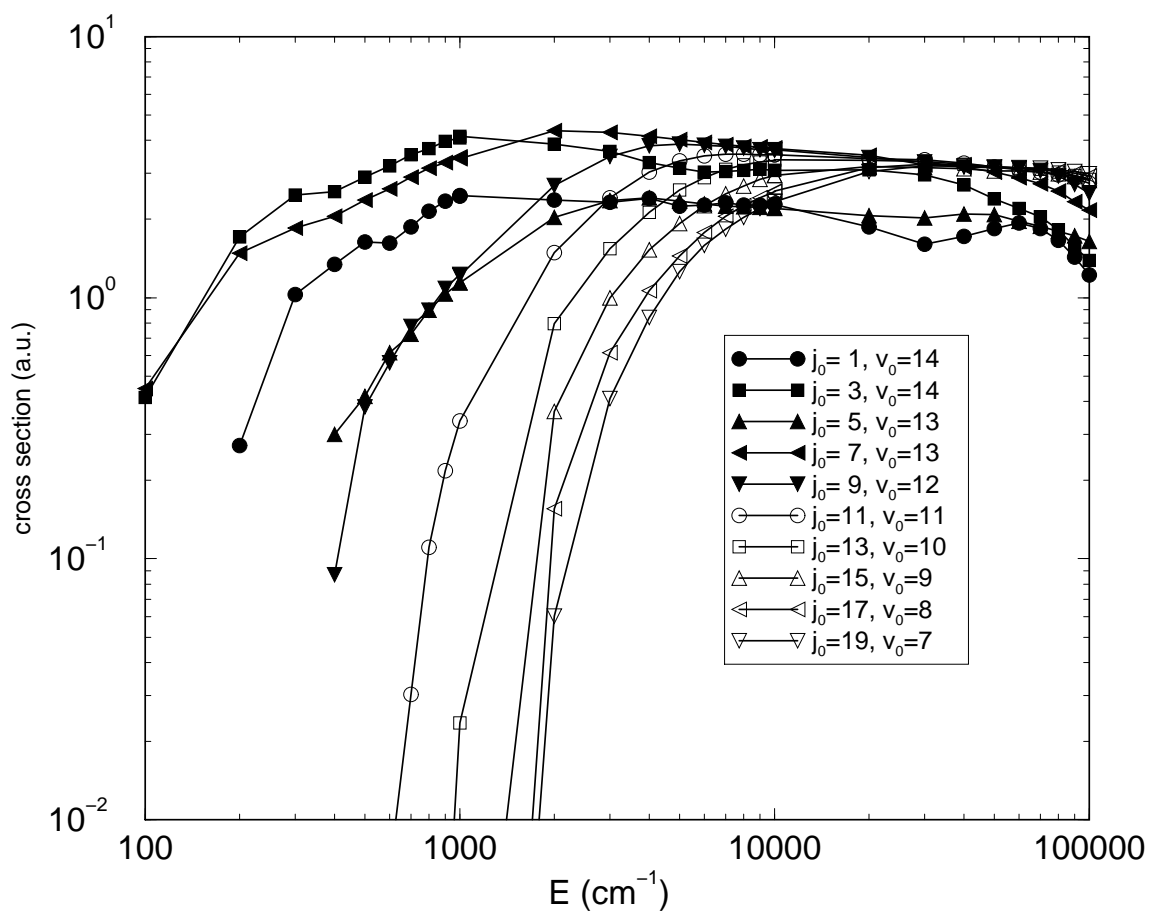


Figure 7: Resonant dissociation cross sections for He collisions with ortho-H₂. Each curve represents a sum of all possible resonant cross sections for the indicated initial state.

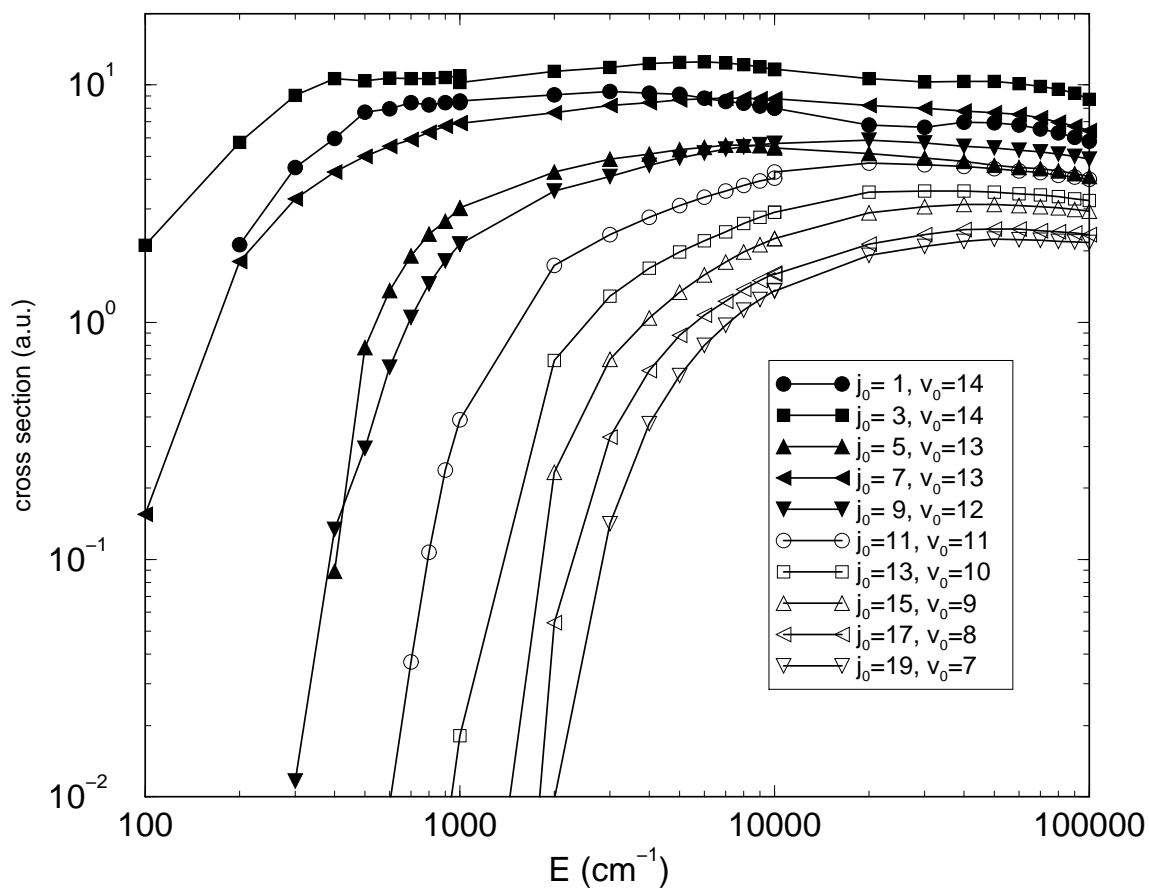


Figure 8: Non-resonant dissociation cross sections for He collisions with ortho-H₂. Each curve represents a sum of all possible non-resonant cross sections for the indicated initial state.

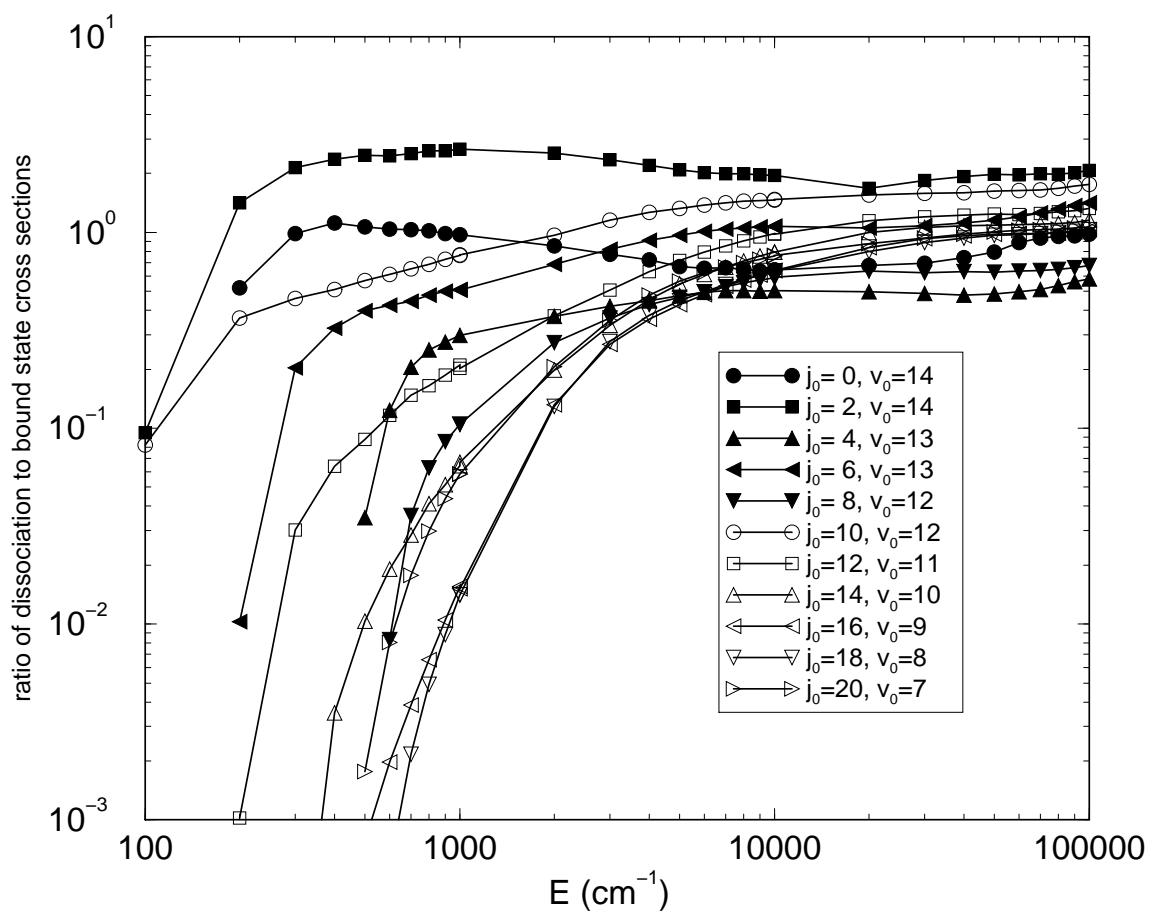


Figure 9: Ratio of the total dissociation cross section to the total cross section for transitions to a bound state for He collisions with para- H_2 .

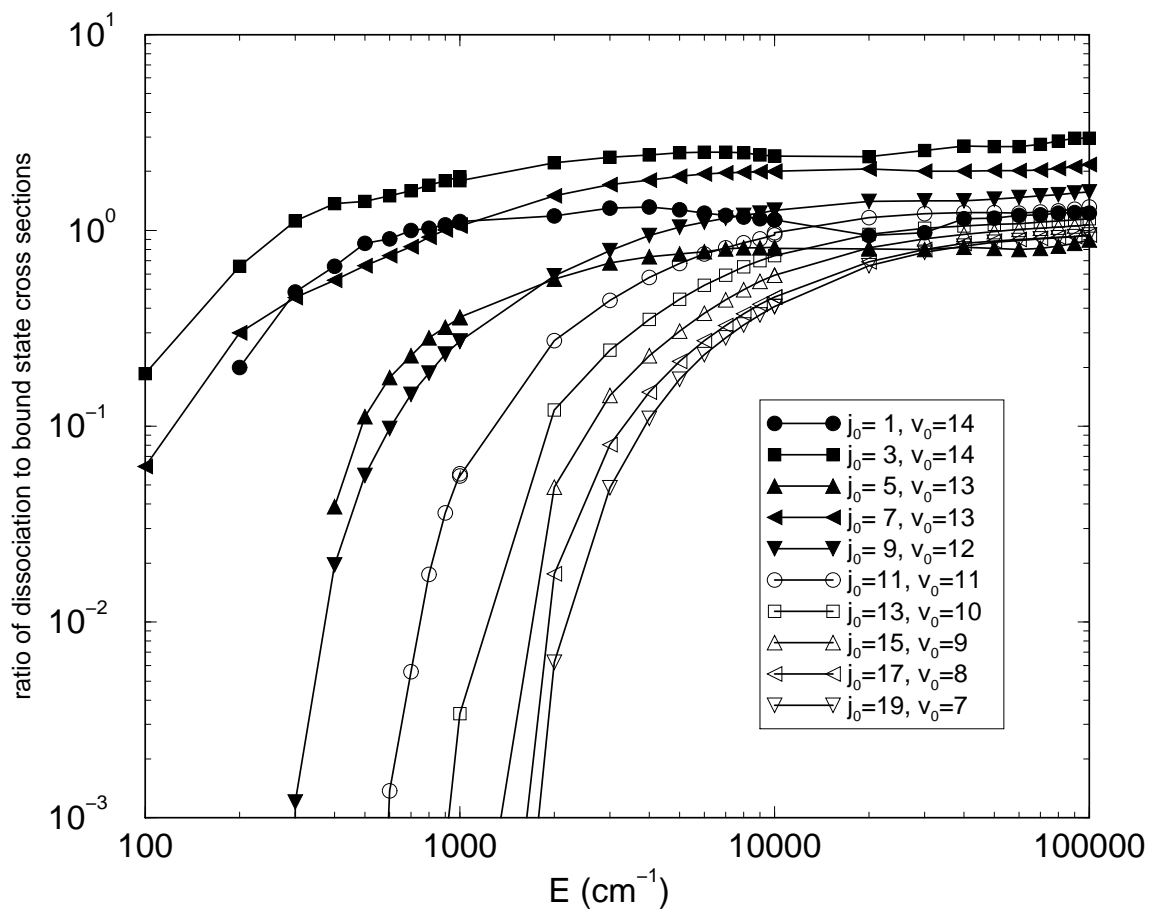


Figure 10: Ratio of the total dissociation cross section to the total cross section for transitions to a bound state for He collisions with ortho-H₂.